http://dx.doi.org/10.1595/205651315X689829 *Johnson Matthey Technol. Rev.*, 2016, **60**, (1), 39–54

JOHNSON MATTHEY
TECHNOLOGY REVIEW

www.technology.matthey.com

Improvement of Noble Metal Based Photocatalysts by Spray Pyrolysis Processes

A review of progress in photocatalytic materials for water treatment applications

By Frédéric Pelletier* and Bénédicte Thiébaut
Johnson Matthey Technology Centre,
Blounts Court, Sonning Common,
Reading RG4 9NH, UK

***Email:** frederic.pelletier@matthey.com

Oxidation technologies and advanced oxidation processes (AOPs) have been regarded as a competitive method for the remediation of persistent pollutants in water. Among AOPs, the use of photocatalysis has particularly attracted interest in recent decades. However, attempts to improve the efficiency of photocatalysts in terms of both enhanced activity and applicability under visible light have proved challenging. In this context, there is a need for processes able to achieve the synthesis of innovative nanostructured materials meeting these criteria with reproducibility and scalability in mind. The aim of this review is to focus on two themes of interest, namely noble metal based catalysts and spray pyrolysis (SP) processes. Several alternative SP methods have been reported and these will be described. The emphasis is placed on the recent use of SP for the synthesis of noble metal/semiconductor nanomaterials and their enhanced photocatalytic activity. Recent innovations in the design of SP processes and their potential to further improve noble metal-based photocatalysts are also examined. Finally, the possibility of using SP processes as a flexible tool to achieve immobilisation of photocatalysts onto substrates and in reactor for real water treatment application is considered.

1. Introduction

With population growth and economic development, there is an increasing demand for potable water. Because of the scarcity of the resource and new sources of contamination, access to clean water is a major environmental challenge worldwide. Moreover, the presence in water of an emerging class of persistent organic compounds such as pharmaceuticals, personal care products and endocrine disrupters that cannot be decomposed by current water treatment technologies, is a major health concern. In search of affordable and efficient processes for water decontamination, photocatalysis has proven to be a good strategy for the degradation of a large range of organic compounds and microorganisms. A great effort has been dedicated to the development of semiconductor-based photocatalysts over the last few decades. Among others, titania (TiO_2) and zinc oxide (ZnO) show the ability to mineralise organic pollutants, are stable, environmentally friendly and cheap. However, the major limitations of these semiconductors are their inability to absorb visible light and the fast recombination of photogenerated holes (h^+) and electrons (e^-) at lattice defects, leading to relatively low quantum efficiency. The improvement of photocatalysts and the design of an efficient catalyst recovery strategy have been reported to be two of the key technical issues that have held back heterogeneous

photocatalysis technology from being implemented at larger scale for water treatment (1).

So far, different strategies have been applied to improve the performance of photocatalysts. These include doping with transition metals (2), anionic doping (3), sensitisation with dye (4), and coupling with carbon nanotubes or graphene (5), low band gap semiconductors (6, 7) or noble metals (8). The latter has been reported as an efficient way to enhance the photocatalytic activity under ultraviolet (UV) light and the resulting materials usually show improved activity towards pollutant degradation compared to the bare semiconductor counterpart (8). Moreover, the ability to absorb visible light by different mechanisms when combined with plasmonic nanoparticles makes these segregated materials attractive for future application. Noble metal supported on semiconductor photocatalysts have been prepared by hydrothermal techniques (9), photodeposition (10), wet impregnation (11), sol-gel (12, 13) and precipitation (14) methods. The production of such supported material has also been carried out by SP processes and this will be the subject of this article.

Hence, the aim of this paper is to update the review recently published by Teoh (15) with a particular focus on: (a) SP-made TiO_2 and to a lesser extent ZnO, combined with noble metals for water application under UV and visible light irradiation; (b) the recent advances in SP processes that may help to develop innovative photocatalysts; and finally (c) the possibility of using SP processes to directly coat substrates with photocatalysts to enable usage in a reactor and offer a practical solution to using this technology in the real world.

2. Spray Pyrolysis Processes

The control of size, chemical phase and phase composition is critical for the design of innovative photocatalysts. SP processes are particularly well suited to produce dried nanostructured materials without requiring post treatment. Many materials including metal oxide nanoparticles, mixed oxides, supported catalysts and doped metal oxides have been produced by SP processes in a very reproducible way (16). As well as allowing access to non-thermodynamic materials, SP processes produce no liquid byproducts, do not require post treatment, are scalable and cost effective. For these reasons, SP processes proved to be excellent methods to produce nanomaterials on a large scale (17–19). The TiO_2 benchmark P25, from Evonik, is a good example of a photocatalyst produced at the industrial scale by vapour-fed aerosol flame synthesis (VAFS). This flame-assisted process consists of feeding a volatile precursor in its gas phase (i.e. titanium tetrachloride ($TiCl_4$)) in a supported flame that initiates the precursor's decomposition to nuclei that further grow through surface growth and coalescence to give nanoparticles. However, in many cases, finding a suitable volatile metal precursor can be a limitation. As an alternative, flame-assisted spray pyrolysis (FASP) techniques such as ultrasonic spray pyrolysis (USP) allow this challenge to be addressed. USP consists of a nebuliser used to produce an aerosol of cheap water-soluble precursor, which is then brought to the external flame using a carrier gas. Alternatively to a flame process, a tube furnace can also be used for the combustion of the precursor (20).

In addition to the flame-assisted methods previously described, SP processes include methods that allow the use of a large range of organometallic precursors dissolved in organic solvent. This alternative approach, including flame spray pyrolysis (FSP) (**Figure 1**), can be described as a self-sustained technique. FSP consists of injecting an organic solution containing metal precursors through a nozzle ignited by a supporting flame fed by a mixture of O_2 and methane or ethylene. The combustion of the solvent allows for the decomposition of the metal precursors and serves as a combustible to sustain the flame.The design of the equipment depends on the application either for particle collection on a glass filter/sock collection system or for the deposition of a nanomaterial on a substrate and more details can be found in existing comprehensive reviews (21, 22).

3. Supported Noble Metals Under Ultraviolet Light

3.1 Theoretical Background

It was reported that photocatalytic performance can be increased by improving the separation of photogenerated charges, hindering charge carrier recombination and facilitating the charge transfer through a heterojunction (23, 24). Deposition of noble metals on a metal oxide semiconductor is a common approach to reach this goal and to further improve quantum efficiency of the photocatalysts. When a hybrid noble metal/semiconductor is irradiated with a UV source and excited by a wavelength of energy above or

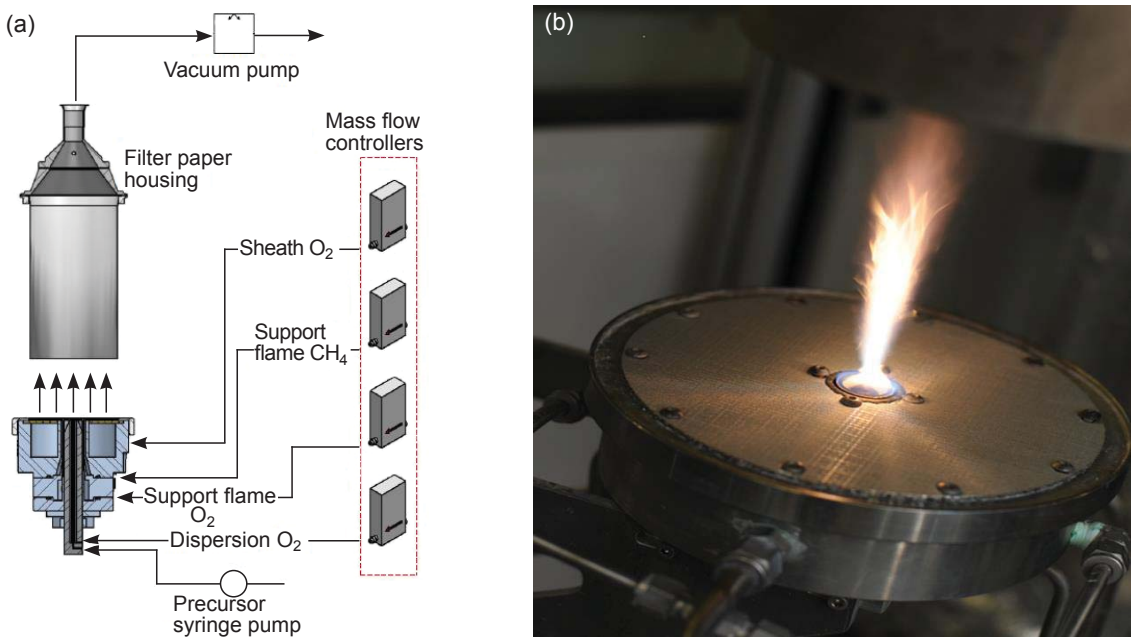

Fig. 1. (a) Schematic of the experimental flame spray pyrolysis setup; (b) picture of the rig during production of nanopowder

equal to the semiconductor's band gap, electrons from its valence band (VB) are transferred to the conduction band (CB) and then further transferred interfacially to the noble metal deposits, where the electrons are trapped. As illustrated below, noble metal deposits accumulate negative charges from the semiconductor's CB and Fermi level shift to a more negative potential close to the CB until it reaches equilibrium (**Figure 2**) (25, 26). This phenomenon results in a better charge separation and an enhancement of the photocatalyst's performance. The barrier formed at the noble metal/semiconductor interface is known as the Schottky barrier and it is worth noting that the height of the barrier can be influenced by the difference of work function between noble metal and semiconductor. From that point of view, platinum is expected to be the best candidate for electron trapping among noble metals (27, 28).

3.2 Noble Metals on Titania Support

Among the literature, reports on the synthesis of noble metals deposited on metal oxides by SP processes

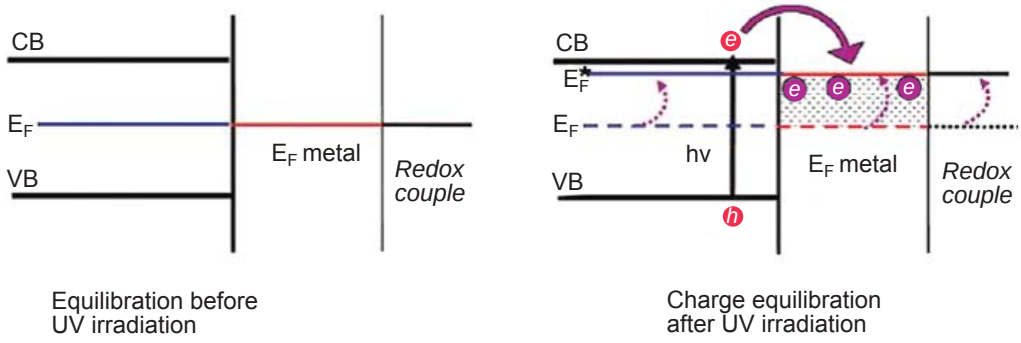

Fig. 2. Equilibration of semiconductor-metal nanocomposites with the redox couple before and after UV irradiation (Reprinted with permission from (25). Copyright (2004) American Chemical Society)

can only be found from the last decade with earlier work from Mädler, Stark and Pratsinis on the gold/titania (Au/TiO_2) and gold/silica (Au/SiO_2) systems (29). When tested for photocatalysis application, these materials usually show promising results in terms of performance compared to commercial benchmarks. The mechanism of their formation relies on the fact that the metal oxide support generally nucleates first at high temperature followed by the sequential deposition of the more volatile platinum group metal (pgm) in the flame either by direct nucleation on the semiconductor or by homogenous nucleation followed by deposition as described by Strobel and Pratsinis (**Figure 3**). This is likely to be applicable to other noble metals due to their high vapour pressure compared to the support materials (30). Teoh *et al.* reported the FSP synthesis of Pt/TiO_2 with high metal dispersion and tuneable size of Pt deposits by varying the Pt loading. A Pt loading of 0.5 at% appears to be optimum for the mineralisation of sucrose under UVA irradiation and showed better performance compared with the benchmark P25.

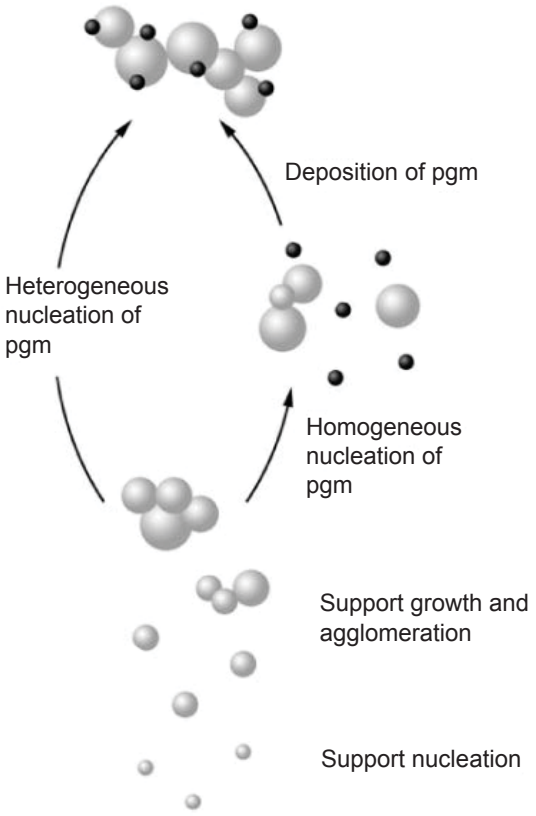

Fig. 3. Mechanism of deposition of pgm on metal oxide substrate in the flame (30)

It was suggested that a lower Pt loading diminishes the number of sites where photogenerated electrons can be efficiently transferred and interact with an electron acceptor in the medium, hence hindering the charge separation and thus the oxidative pathway through photogenerated holes. At higher Pt loadings, in addition to the screening effect of Pt deposits preventing the optimum irradiation of TiO_2, it was suggested that the presence of an increasing amount of negatively charged Pt may improve the recombination of photogenerated holes leaving fewer holes available for photooxidation and hindering photocatalytic activity as a consequence (31). It is worth noting that the formation of nanoparticles in a highly oxidative flame results in nanostructured materials with noble metal deposits in an oxidised state. This was further investigated, as 0.5 at% Pt/TiO_2 was analysed by X-ray photoelectron spectroscopy (XPS) before and after photocatalytic mineralisation of different organic substrates, namely formic acid, phenol and methanol, demonstrating the influence of the Pt oxidation state on the kinetics of the photocatalytic reactions (32).

Tiwari *et al.* have synthesised Pt/TiO_2 with a setup involving a flame fed with titanium isopropoxide (TTIP) and acetylacetonate-based aerosols and found that the optimum loading for methyl orange degradation in aqueous phase under UVA lies between 0.5 wt% and 1 wt% Pt, which is consistent with the results described above. Interestingly, bare TiO_2 contains a mixture of anatase and rutile, and in this flame-assisted procedure the addition of Pt dopant led to the suppression of the total rutile fraction while in the case of the FSP-made materials presented above, X-ray diffraction (XRD) showed no disappearance of rutile phase with the addition of Pt. The doping of TiO_2 with 0.5 wt% palladium was also investigated and appeared to be detrimental to the photocatalytic activity, the methyl orange degradation rate being even lower compared to bare TiO_2. It was suggested that the low performance of Pd/TiO_2 could be either due to the nature of the dye or to the fact that 0.5 wt% Pd may be above the optimum loading for methyl orange degradation. The oxidation state of Pd may also have an influence but has not been the object of further study. A bimetallic composite 0.5 wt% Pd-Pt/TiO_2 was synthesised and showed an intermediate photocatalytic activity compared to Pd/TiO_2 and Pt/TiO_2 (33).

Recently, an attractive strategy has been employed by Paulauskas *et al.* to combine doped 0.4 at% Pt/TiO_2 with 14 at% Al and 7 at% Sn to further improve

the degradation rate of methyl orange. A series of nanocomposites: platinum-aluminium/titania (Pt-Al/TiO_2), platinum-tin/titania (Pt-Sn/TiO_2) and their undoped derivatives, respectively 14 at% Al/TiO_2 and 7 at% Sn/TiO_2, were prepared by FSP. The results showed that among Pt/TiO_2-based photocatalysts, Pt-Sn/TiO_2 shows the highest degradation rates compared to Pt/TiO_2 and the commercially available benchmark P25 (34).

As an alternative to flame assisted methods, Haugen *et al.* used SP equipment for the atomisation of an aqueous solution of precursors followed by calcination in a tube furnace between 800ºC and 1000ºC at short residence time to produce TiO_2, Ag/TiO_2 and Au/TiO_2. In some cases, the materials were further calcined for 3 h between 550ºC and 900ºC. Methylene blue was used to assess the photocatalytic activity under UV light irradiation and the results showed that the as-prepared TiO_2 photocatalysts containing a non-negligible quantity of amorphous TiO_2 show a similar activity to the reference P25. Despite being more crystalline, the calcined materials showed a lower photocatalytic activity. It was suggested that the higher amount of rutile in the as-prepared samples could be responsible for this trend. Interestingly, in this study, no improvement of photocatalytic activity was found in the case of noble metal/TiO_2 materials. It was suggested that the rather large size of Au and Ag crystallites in the calcined materials (20–30 nm and 5 nm respectively) were acting as recombination centres (35).

3.3 Noble Metals on Zinc Oxide Support

Compared to TiO_2, the synthesis and testing of ZnO-based photocatalysts by SP methods has been studied to a lesser extent. Height *et al.* compared the performance of Ag/ZnO nanomaterials prepared by FSP and wet impregnation methods. On a mass basis, FSP-made nanomaterials showed higher photocatalytic activity toward discolouration of methylene blue under UV irradiation compared to wet-made materials and the TiO_2 P25 benchmark. For both synthesis methods, a Ag loading of 3 at% was found to be optimal for the conversion of methylene blue. For FSP-made nanomaterial, the photocatalytic performance was increased when the ratio of the liquid precursor feed rate to the O_2 dispersion gas flow rate was highest. A higher liquid to gas ratio increases the flame height and the residence time of the nanomaterial at higher temperatures, thus resulting in materials with fewer crystal defects as supported by XRD and ultraviolet-visible (UV-vis) absorption measurements (36).

Recently, Siriwong *et al.* synthesised a series of Pd-doped ZnO materials by one-step FSP. Photocatalysts were tested for the degradation of three different substrates under UV light irradiation and the results showed that a loading of 0.5 at% Pd was the optimum for the degradation of methanol, glucose and sucrose (37). Pawinrat, Mekasuwandumrong and Panpranot synthesised Pt/ZnO and Au/ZnO by FSP and tested their activity on the degradation of methylene blue under UVA irradiation. Photoluminescence emission studies showed that the recombination rate of Au/ZnO was lower than for Pt/ZnO; these results were consistent with better photocatalytic performance of Au/ZnO compared to Pt/ZnO. The low performance of the latter was in accordance with the literature and was attributed to the ohmic nature of the contact between Pt and the semiconductor ZnO resulting in the poor ability of Pt deposits to store photogenerated electrons hence to increase electron-hole separation lifetime as occurs in the Pt/TiO_2 system (38).

4. Supported Noble Metals Under Visible Light

4.1 Theoretical Background

In addition to increasing charge carrier separation and improving overall quantum yield, decorating a semiconductor with plasmonic nanoparticles such as Au and Ag is also beneficial for photocatalysis as it allows visible light absorption. Due to the ability of plasmonic noble metals to concentrate and scatter photons, the absorption of TiO_2 can be extended to visible light through localised surface plasmon resonance (LSPR). LSPR is the strong coherent oscillation of the plasmonic particle's free electrons when in phase with the electric field of incident light. **Figure 4** shows an

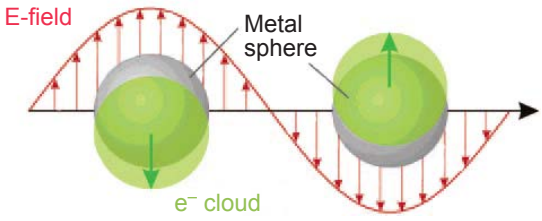

Fig. 4. Illustration of a localised surface plasmon (Reprinted with permission from (39). Copyright (2003) American Chemical Society)

illustration of LSPR where light interacts with a particle smaller than its wavelength. The resulting localised plasmon oscillates around the particle at a certain frequency (40).

When a plasmonic nanoparticle/semiconductor nanostructure is exposed to visible light, different mechanisms may take place:

(i) the electron transfer between the plasmonic nanoparticle and the conduction band of the semiconductor can be induced by LSPR in a similar mechanism to sensitisation
(ii) when the electronic transfer is diminished due to non-conductive separation between the plasmonic metal and the semiconductor, LSPR may induce an enhancement of the electromagnetic field near the surface of the plasmonic particle that increases the charge carrier formation in the nearby TiO_2 region
(iii) the photon's path length may be increased at the surface of the semiconductor by the scattering of noble metal nanoparticles.

Enhancement of the absorption is influenced by the loading, the size and the shape of the plasmonic particles. An extensive coverage of plasmonic photocatalysis can be found in comprehensive reviews (8, 28, 41).

4.2 Silver and Gold on Titania Support

Compared to coimpregnation and deposition-precipitation techniques, SP processes can provide benefits for the design of supported catalysts both in terms of size distribution and uniformity of deposits (42). This could be an advantage for the design of visible light active photocatalysts. However, to the best of our knowledge, only a limited number of plasmonic photocatalysts made with SP processes have actually been studied under visible light irradiation for the photodegradation of pollutants. A few examples of these materials have however been reported for other applications under visible light.

This includes work undertaken by Gunawan *et al.* in which FSP-made Ag/TiO_2 could be used as a reversible photoswitch for antimicrobial applications. The application relies on control of the oxidation state of silver. Exposure of Ag^0 deposits to visible light (>450 nm) allows the electrons to migrate to the TiO_2 support through LSPR hence oxidising Ag^0 to Ag^+. The process is reversible under UV light irradiation (43). This work gives a particular insight into oxidation state and leaching behaviour of FSP-made Ag/TiO_2 that is relevant for potential photodegradation applications under visible light irradiation. The leaching of noble metals has been reported in several articles, especially in the case of Ag/TiO_2 photocatalysts. This is a matter of concern for sustainable water purification applications since it could be the cause of a loss of photocatalytic performance over time and the release of toxic Ag^+ into the water stream (44, 45).

Interestingly, some studies suggest that a combination of both Au and Ag plasmonic metals could show improved stability against surface oxidation and hinder Ag^+ leaching. First, Hannemann and coworkers demonstrated by complementary analysis, including extended X-ray absorption fine structure (EXAFS) spectroscopy, that Au and Ag could form alloyed nanoparticles by FSP synthesis. X-ray absorption near edge structure (XANES) spectra could give information on Ag oxidation state and suggested that Ag was slightly more oxidised in the absence of Au (46). In addition, a recent study investigating LSPR and leaching of FSP-made Ag-Au nanoalloys confirmed this trend and showed that Ag^+ leaching was minimised with an alloy containing over 50 at% Au (47). The $Au-Ag/TiO_2$ system has been little studied for water application, although a few examples exist in the literature. This includes one study on $Au-Ag/TiO_2$ nanomaterials made by microemulsion that show promising results for the degradation of phenol under visible light irradiation compared to their monometallic counterparts, but there was no mention of potential Ag leaching (48).

These examples show that SP routes have potential for the production of photocatalysts active under visible light irradiation.

5. Modified Flame Spray Pyrolysis Techniques

Progress has also been made toward the development of the FSP technique in order to allow the fine-tuning of size, chemical composition and architecture of the nanostructured materials. Changing the catalyst characteristics would allow for the optimisation of their activity.

5.1 Quench Cooling Technique

It is highly desirable to be able to tune the size and shape of a noble metal on a semiconductor substrate as these parameters greatly influence the absorption of visible light. In the case of plasmonic deposits, the scattering mechanism and the overall photocatalytic activity

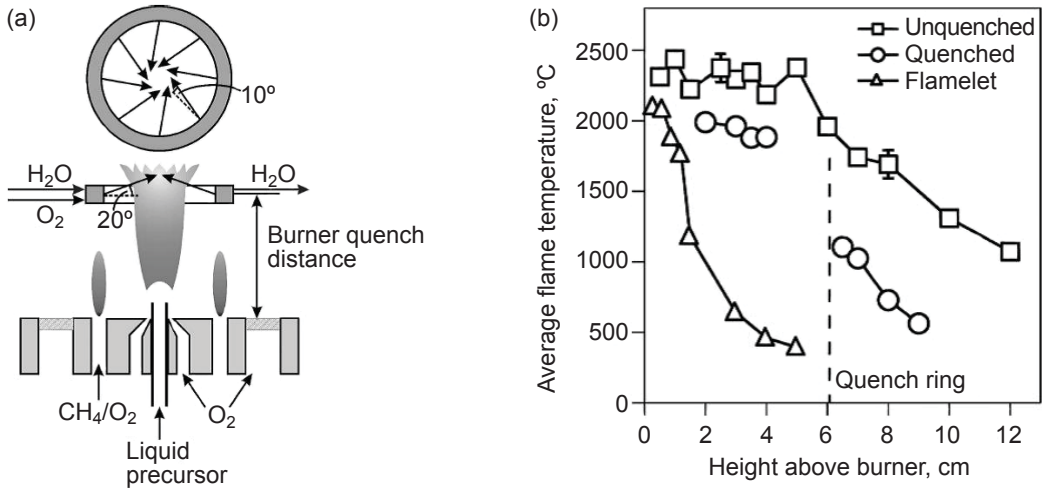

Fig. 5. (a) Burner equipped with a quench cooling device; (b) temperature profiles of the flame spray at standard condition (i.e. unquenched), under quenched condition with a quench ring located at 6 cm above the burner and without precursor feed (49) (Reproduced with permission from Cambridge University Press)

may be adjusted in this way. Schulz *et al.* developed a quench-cooling device to independently tune the TiO_2 support and the deposits of Pt nanoparticles on its surface. The device consists of a ring placed axially around the flame, adjustable to 2 to 12 cm from the burner outlet of a FSP rig (**Figure 5(a)**). A cooling gas is injected from the ring to quench the flame temperature at an early stage (**Figure 5(b)**). By tuning the distance between the burner and the quenching ring, it was possible to modulate both the dispersion and the average diameter of the Pt nanoparticles. The benefits are particularly interesting at high Pt loading (up to 10 wt%) since the average Pt diameter is better controlled compared to unquenched experiments (49).

In the work conducted by Tiwari *et al.*, a similar quenching approach to tune the specific surface area of 1 wt% Pt/TiO_2 was investigated. Results show a decrease of the surface area from 88 to 74 $m^2 g^{-1}$ when using a quenching ring located at 5 and 10 cm from the burner respectively. Compared to the experiments described above, the same precursor (TTIP) was used as a Ti source but in this latter study, the precursor was introduced in the vapour phase rather than as liquid droplets for FSP. Consequently, the mechanisms of nanoparticle formation, described in **Figure 6** (22), may yield different particle characteristics. The authors investigated the influence of the quenching ring position toward the photocatalytic performances. The photocatalysts obtained were assessed under UV irradiation and results show that the rate for methyl orange degradation decreases with the distance at which the quenching ring is located from the burner, the highest rate being when the ring is located at the lowest position (5 cm). The authors demonstrated that this trend originates from the nanomaterials physical properties and showed that by taking surface area into account the modified rate constants were similar (33).

Alternatively, to provide cooling gas, a second injection ring can be used to feed the flame with a volatile precursor to dope the semiconductor or alternatively to achieve a partial reduction by feeding with H_2.

5.2 Routes to Modified Titania

Tuning the band gap of a semiconductor is key to allow a photocatalyst to extend its absorption to the visible light region. However, the introduction of a foreign cationic dopant in the semiconductor framework may act as a recombination centre and hinder photocatalytic activity (50). As an alternative, the synthesis of sub-stoichiometric titania (TiO_x) which contains oxygen vacancies, VO-Ti^{3+}, appears to be a good way to achieve visible light harvesting without including any impurity elements usually required to induce this effect (51). Recently, black and blue coloured defective titania nanomaterials were successfully synthesised using different routes including solvothermal process (52, 53), crystallisation/reduction process (54)

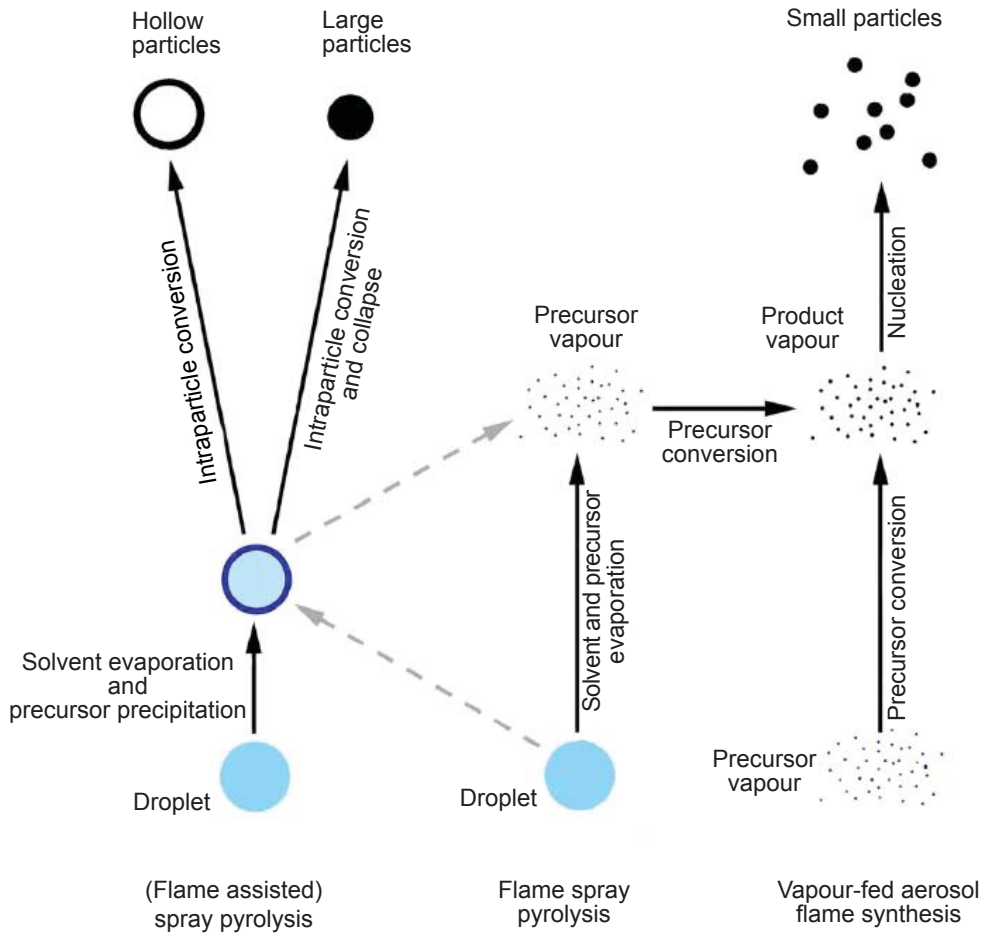

Fig. 6. Mechanism of formation of particles during spray pyrolysis processes (22) (Copyright © 2006 Koninklijke Brill)

and spark plasma sintering (55). Compared to pristine or commercial TiO_2, the improvement of the photocatalytic efficiency under visible light irradiation either for the degradation of dyes or for the selective photooxidation of methylcyclohexene to ketones were achieved in every case.

Modified FSP technique can also be run under controlled conditions to produce nanomaterials under rich or lean O_2 environment. It has been demonstrated that by closely controlling the O_2/N_2 atmosphere around an enclosed flame, the polymorphic anatase/rutile ratio could be finely tuned. In the most anoxic conditions (i.e. sub-stochiometric O_2 content), oxygen vacancies were induced and promoted the highest content of TiO_2 rutile, up to 94 wt% (56). Using a combination of anoxic conditions and a quench cooling ring, Pratsinis and coworkers demonstrated the possibility of inducing oxygen vacancies and producing blue TiO_2 in one step. These particles showed long-term colour stability suggesting that the defects are located both inside and at the surface of the particles (57, 58). As an alternative to the quench cooling process, Huo *et al.* synthesised surface doped TiO_2 with Ti^{3+} by reducing the particle surface *in situ*. In a one-step VAFS process, $TiCl_4$ was brought to the flame with a N_2 flow and was ignited by a supported flame; a second injection ring placed 15 cm above the nozzle introduced H_2 above the flame to generate reduced Ti^{3+} near the surface. The resulting blue titania showed enhanced photocatalytic activity under visible light irradiation compared to P25 and pristine TiO_2 (59). However, the stability over time of such a reduced surface could be of concern for practical applications.

Another approach involving noble metal and taking advantage of the ‘strong metal-support interaction’ (SMSI (60)) effect has been recently undertaken

by Fujiwara *et al.* to produce sub-stoichiometric $AgTiO_2$-TiO_x by FSP in a single step under low oxidative flame conditions. The resulting 'black titania' consists of the distorted crystalline TiO_x phases (Ti_4O_7 and Ti_3O_5) on Ag nanoparticles supported on TiO_2. According to the authors these materials were obtained as a result of fine control of the O_2 flow against precursor feed rate and the presence of a large amount of intermediate combustion products during the synthesis, allowing the reduction of TiO_2 to TiO_x. The SMSI between Ag and TiO_2 induces the formation of a TiO_x overlayer that covers, at least partially, the Ag nanoparticles. Interestingly, the plasmonic resonance band due to Ag^0 could not be observed by diffuse reflectance absorption and this was attributed to the SMSI suggesting that the contribution of the plasmonic nanoparticle is minimal. Consequently, improved visible light absorption and photocatalytic activity against Cr^{6+} reduction and methylene blue degradation were attributed to TiO_x at the surface of Ag (61).

5.3 Anionic Doping by Flame Spray Pyrolysis

The doping of TiO_2 with non-metallic elements, such as fluorine and sulfur, is of great interest since it was reported to hinder charge carrier recombination and to increase electron lifetime hence improving the photocatalytic activity of TiO_2-based material (3, 62–67). Moreover, nitrogen doping can enhance the absorption of visible light (68–70). Common wet chemistry methods for anionic doping make use of post thermal treatment that affects chemical properties and specific surface area (SSA) (71). In addition, reproducibility is a matter of concern. FSP can achieve anionic doping in one step either by direct injection or by the use of a second injection ring. As an example, Jiang, Scott and Amal reported the F-doping of TiO_2 by direct injection of F and titanium precursors by FSP. An enhancement of photocatalytic activity toward degradation of acetaldehyde in the gas phase under UV irradiation was reported (72). Recently, Chiarello *et al.* co-doped Pt/TiO_2 with F in a single step also by direct injection of precursors. Compared to its F-free counterpart, the resulting F-doped material appears to be more efficient to photocatalytically produce H_2 from methanol under UV irradiation. It is worth noting that in this particular case, the ideal amount of F is 5 at% and an increase above 10% is detrimental to the photocatalytic activity due to the formation of structural defects improving charge carrier recombination (73).

Due to the high enthalpy of the flame and the fast reaction rate, doping with nitrogen or sulfur precursor is difficult to achieve by direct injection as the dopant element is likely to be oxidised to nitrogen oxides (NOx) and sulfur oxides (SOx). It is therefore desirable to introduce the precursor downstream at a greater distance from the burner where the temperature is lower according to the temperature profile of a FSP unquenched flame (**Figure 5**) (49). With the aim of achieving the preparation of nitrogen-doped TiO_2 by FSP in a single step, Huo *et al.* first produced TiO_2 by FSP and introduced a solution of ammonia above the flame by means of a spray nozzle (**Figure 7**). The resulting material consists mostly of the anatase polymorph (90.8%) and XPS results suggest that the presence of nitrogen is due to the replacement of oxygen atoms by nitrogen near the TiO_2 surface. The introduction of nitrogen increases the visible light absorption as shown by UV-vis spectroscopy. This material was not tested for water application but the study of dye sensitised solar cell (DSC) performance demonstrates a decrease in the charge recombination rate for the anionic doped TiO_2 (74).

These engineering changes to the flame spray process have shown that complex materials can be obtained in one step yielding superior activity and

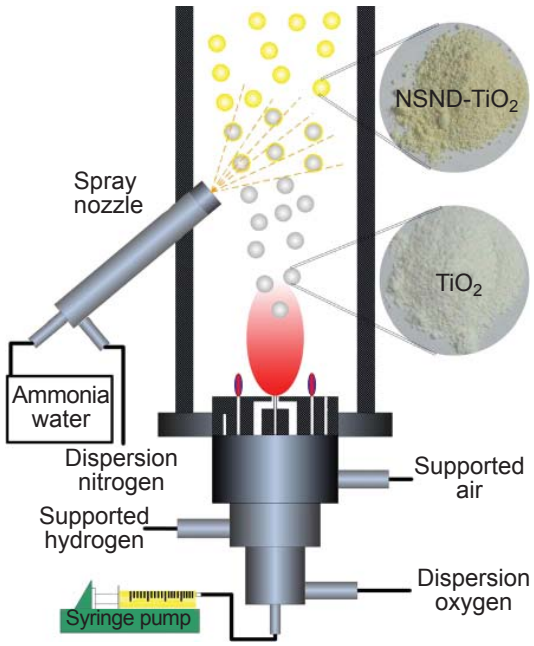

Fig. 7. Schematic setup for N-doped TiO_2 nanoparticles (Reprinted from (74). Copyright (2014), with permission from Elsevier)

demonstrating the importance of the technique to deliver unique catalysts. Further complexity to the process was developed with the use of two separate nozzles to bring more flexibility to FSP and to control at which steps of nucleation or growth a noble metal can encounter the metal oxide semiconductor in the flame.

5.4 Double Flame Spray Pyrolysis

Even better control of size and chemical composition of a noble metal deposit on a support can be achieved by spraying two solutions of precursors in two separate FSP nozzles. Complex heterostructures such as platinum/barium/alumina and cobalt/molybdenum/alumina can also be obtained in this way (**Figure 8**) (75, 76). The technique, known as double FSP, allows the particle growth of the catalyst or material components to be individually tuned, and mixing to be controlled at different stages by adjusting the geometry and precursor mixtures for each individual nozzle. In the Pt/Ba/Al_2O_3 system, the location of Pt and Ba deposits on the Al_2O_3 support are crucial factors for NOx storage-reduction (NSR) and a double nozzle introduces greater flexibility for the design of such a catalyst. Indeed, the use of a single nozzle leads to the dispersion of amorphous Ba material throughout Al_2O_3 (**Figure 9(a)**), while the use of two nozzles allows the formation of both Al_2O_3 and Ba species in their respective flames before mixing occurs, thus leading to the synthesis of the desired crystalline barium carbonate ($BaCO_3$) dispersed on Al_2O_3 nanoparticles (**Figure 9(b)**). In addition, it was demonstrated that the internozzle distance has a strong impact both on the amount of Ba in the form of $BaCO_3$ and on the Pt dispersion as both values decrease with decreasing internozzle distance due to the influence of the second flame's heat contribution at shorter distance (65).

A recent study focused specifically on the impact of the nozzle arrangement. When there is large spacing between nozzles (20 cm) simulation and Fourier transform infrared (FTIR) measurements of the temperature profile along the flame axis show that there is no increase in the flame temperature either close to the burner or at the intersection of both flames, suggesting that the temperature profile is similar to that of a single flame. On the other hand, when the distance decreases to 10 cm, the temperature increases by up to 300 K compared to a single flame configuration possibly due to a decrease of the effect of cooling by the surrounding air at the point of intersection. However, according to XRD results, the increase in the flame temperature has no effect on the crystallinity and anatase/rutile ratio of titania.

H_2 chemisorption measurements show that the dispersion of Pt deposits is lowered by the double flame arrangement compared to direct injection of both precursors in a single flame. This work clearly emphasises the importance of aerosol mixing in the synthesis of the desired noble metal supported on metal oxide nanostructured material (77). From a design of photocatalyst point of view, the advantage of double FSP lies in the possibility to tune the TiO_2 physicochemical properties in a separate flame without affecting the size and the dispersion of Pt deposits on the support.

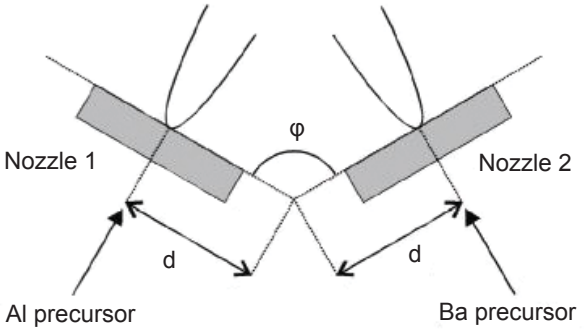

Fig. 8. Scheme of the geometric arrangement of a double FSP set up (Reprinted with permission from (75). Copyright (2006) American Chemical Society)

6. Designing Immobilised Photocatalysts

Many experimental studies of photocatalysis reported in the literature are slurry-based whereby a TiO_2 based catalyst is suspended in an aqueous media to be tested for the photodegradation of pollutants under a radiation source. For large scale applications, the design of photoreactors for slurry and immobilised systems has been the subject of various papers and reviews (1, 78–80). Although advances in slurry-based reactors have been reported (81), the post separation difficulties associated with the powder form of the TiO_2 catalyst from the treated water often remains a challenge. To that effect, various methods have been employed to immobilise the photocatalysts and many techniques have been used to form thin films onto a wide range of substrates including sol-gel, chemical

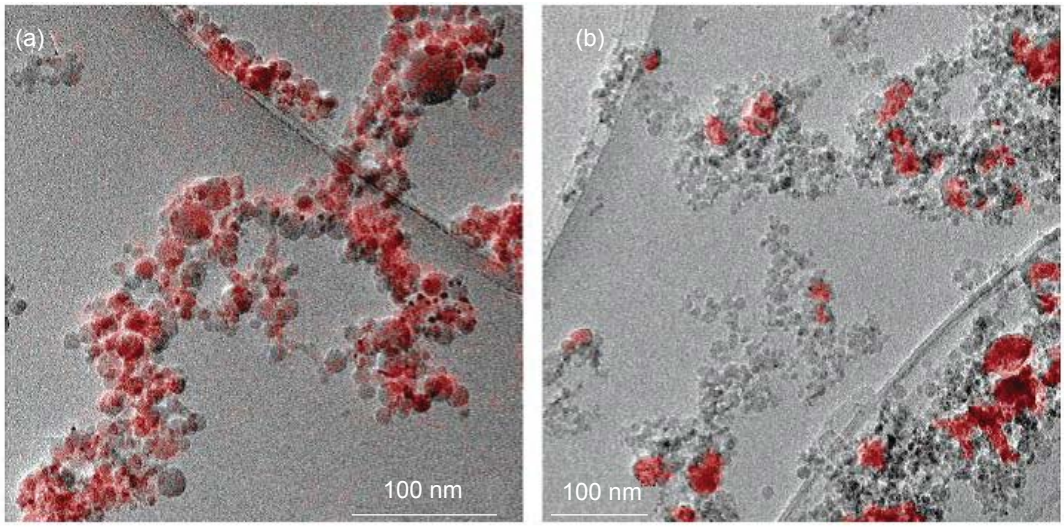

Fig. 9. Transmission electron microscopy (TEM) pictures of Pt/Ba/Al_2O_3 made with: (a) one nozzle; (b) two nozzles. The red areas indicate the presence of Ba (Reprinted with permission from (75). Copyright (2006) American Chemical Society)

vapour deposition, sputtering, pulsed laser deposition, electrospray deposition and SP (82–94).

6.1 Flame Spray Pyrolysis Deposition

One recent review summarises the methods for the preparation of nanoscale TiO_2 films for water remediation applications (95). FSP is the method of interest in this review. This technique allows a flexible and scalable process for synthesis and deposition of thick nanostructured coatings on large surfaces in a very short time. The reagents are pyrolysed prior to deposition onto the substrate. The precursors are dissolved or suspended in a liquid medium and sprayed by gas or ultrasonic assisted means. The evaporation and decomposition of the reagent solutions are carried out either by self-sustained spray combustion with an organic based solution ignited by a pilot flame or, for an aqueous based solution, an external heat source such as a H_2 flame is supplied. The products from such processes are often collected as powders although there are also reports on their direct deposition onto a wide range of substrates (96, 97).

The chemical (98) and mechanical strength of such films in the reactor environment is critical for ‘real-life’ applications. Direct FSP deposition tends to yield low mechanical stability films; however *in situ* film annealing with an impinging flame produced much improved strength (99, 100). Alternatively the substrate may be heated during the deposition to provide a degree of annealing and thus mechanical strength (101). Depending on the substrate temperature, a porous film is either preserved or collapses into more compact structures by sintering (102). A modification of the FSP process was also reported recently in which it was coupled with supersonic expansion to allow deposition under mild conditions, avoid a high substrate temperature and obtain a coherent film (103).

A small number of reports have been found regarding thin films containing noble metals and these are reviewed below. Keskinen *et al.* reported the H_2/O_2 FASP of TiO_2-Ag thin film on steel and glass plates. A range of flame to substrate distances and deposition times were studied together with subsequent deposition of TiO_2 and Ag or direct deposition of both components at once. Analysis revealed that metallic Ag is highly enriched and sintered on the surface of the TiO_2 crystallite in the two-step method compared to the one-step method which yielded more dispersed discrete Ag nanoparticles. The TiO_2 films were made of mostly anatase and the crystallite size was in the region of 10 nm. Grain size decreased with Ag doping. The films were tested for the photodegradation of stearic acid. The Ag-TiO_2 film prepared in a single step showed a higher value of the formal quantum efficiency (FQE) compared to TiO_2. The films were then wiped and retested. The activity dropped dramatically and this was associated with removal of the powder demonstrating the low mechanical strength of such a deposition technique unless some annealing

treatment is carried out, as described in the previous paragraph. After removing the loose particles, the thin film produced closest to the nozzle showed the highest activity. According to the authors, the shorter collection distance during deposition might have made the particles more adherent to the substrate as the film had been exposed to a higher temperature (104).

Mädler *et al.* reported the formation of a Pt-SnO_2 thin film by FSP of Pt and Sn precursors directly deposited onto Al_2O_3 sensor substrates by thermophoresis. They describe the advantage of using this technique over other deposition methods since it can deliver one-step high-temperature synthesis of single or doped materials, defined as functionalised and without the need for post-annealing as in conventional SP.

The films were described as porous (up to 98% porosity) with tin oxide grain size ~10 nm. The thickness of the films could be varied from 9 to 40 μm using different deposition times without affecting the high porosity. Pt doping did not affect the SnO_2 grain size, crystallinity or the porous film structure. These films were tested as CO sensors (105).

Thybo *et al.* flame sprayed a metal precursor solution made of gold-triphenylphosphine nitrate and Ti-tetraisopropoxide in a mixture of tetrahydrofuran and isooctane to produce a 1 wt% Au/TiO_2 catalyst, which was directly deposited onto a range of substrates usually used in the fabrication of microfluidic reactors, including Si, Ti, Al, Si_3N_4 and H:Si. The substrate holder was cooled at different temperatures and this seemed to influence the deposition rate. Photolithography was used to make patterns with a resolution better than 100 μm, indicating that the flame spray technique is suitable for the functionalisation of micron sized channels used in microfluidic systems. An optimal nozzle to support distance was determined to allow uniform radial deposition of catalyst onto the support.

The surface area of the films was about 350 m^2 g^{-1}; higher than those obtained from powders collected on a filter. This is most likely due to the quenching of the particles deposited nearer the tip of the flame on a cooled substrate which would reduce the particle collisions and coalescence. The adhesion of films was not quantitatively determined and it is difficult to ascertain the actual strength of the bond of the thin films onto the substrates. The catalyst coated substrate incorporated into a microfluidic system was tested *in situ* for the gas phase oxidation of CO to CO_2 (106).

This last example shows that FSP could be an efficient method to prepare reactors which could be adapted to be illuminated with an appropriate light source and used for the continuous decontamination of water wastes.

6.2 Spray Pyrolysis Deposition

An alternative process to FSP is the SP method which is a versatile low cost technique that also enables deposition onto large areas. A liquid is atomised by gas, ultrasonic or electrostatic means. The formed droplets travel to the substrate during which time the solvent may evaporate. Once the shrinking droplets reach the surface of the hot substrate, the droplets undergo pyrolytic decomposition. The volatile byproducts and solvents escape in the vapour phase and sintering and crystallisation of the clusters of crystallites yield a film. There are many parameters controlling the quality of the thin films and these are summarised in reviews (107, 108). For noble metal containing thin films prepared by this method, literature reports have been found to include either simultaneous deposition or subsequent deposition of the semiconductor and the noble metal (109). These are reported for other usage than photocatalysis for degradation of water pollutants; however they are introduced in this review as they may be a good source of interesting materials for photodegradation applications. Tarwal and Patil prepared Au-ZnO thin films onto indium tin oxide (ITO) coated glass substrates by spraying an aqueous solution of silver nitrate and zinc acetate together onto the pre-heated substrate at 450ºC. Upon addition of Ag at various loadings, the thin films become generally more compact and uniform with smaller crystallites. The authors describe the optical characteristics of the thin films using UV-vis spectroscopy with a band edge ~380 nm for pure ZnO and the presence of an absorption peak within the range 530–570 nm due to the presence of Ag nanoparticles. The transmittance is somewhat decreased in the films which contain Ag, possibly due to grain boundary scattering. The photoelectrochemical properties of the thin films were studied and improvements in performance of the Ag-ZnO thin film over that of pure ZnO were attributed to surface plasmon resonance enhanced absorption phenomena (110).

Mohite and coworkers developed Au-doped TiO_2 thin films by spraying non-aqueous based solutions of Au and Ti onto a heated substrate at 450ºC. The Au doping was varied from 1 to 4 at%. The process parameters and optimum Au doping were determined using photoelectrochemical methods. The Au doped

TiO_2 thin films exhibited better photoresponse than that of pure TiO_2 and the best performance was obtained with 3 at% Au. Interestingly, the XRD analysis revealed that at higher loading to 3 at%, the peak intensity of Au decreases while the TiO_2 peak shifts due to the incorporation of Au in the TiO_2 matrix.

The degradation effect on benzoic acid was claimed to be 49% higher in 3 at% Au-doped TiO_2 than in the pure TiO_2 thin film photoelectrodes, although no data was presented for these. The enhanced photoactivity was attributed to the widening of the response of the photocatalyst into the visible region as a result of Au doping. It was also reported that Au doped TiO_2 could be reused for five cycles of experiments without the need for a post-treatment while the degradation efficiency was retained (111).

Acik *et al.* used a preparation in which they first deposited the TiO_2 by a sol-gel chemical spray pyrolysis method whereby a solution of titanium(IV) isopropoxide and acetylacetone in ethanol was pulverised onto the preheated glass substrates at a growth temperature of 400ºC.

Au nanoparticles were then formed by spin coating a solution of chloroauric acid ($HAuCl_4$) onto the TiO_2 films; the resulting composites were then dried and finally annealed. The particle size of the Au particles was found to increase with increasing Au concentration. The TiO_2 films were about 120 nm in thickness and made of a mixture of amorphous and crystalline anatase. The authors planned to adapt the preparation of these Au nanoparticles TiO_2 thin films for thin plasmonic coatings for photovoltaic applications (112).

The same authors also described more recently the preparation of Au doped thin TiO_2 films by spraying both components directly onto a heated substrate. The Au content in the thin films was determined and interestingly, the [Au]/[Ti] ratio decreases with increasing deposition temperature from 260 to 300ºC and no Au was detected in films prepared at deposition temperature of 400ºC. The thin films were finally annealed at 400ºC and no loss of Au was observed. The annealing at 400ºC has a minor influence on the size of the Au nanoparticles.

The UV-vis spectra were studied and showed a red shift of the surface plasmon resonance band from 570 to 620 nm. This was associated with the increase in the refractive index of the TiO_2 matrix (113). These coatings could be of interest for photocatalysis but were not tested for this particular application.

It is clear from this section that interesting noble metal containing materials and thin films can be developed. However, further work is needed to investigate the adhesion and lifetime of these thin films for the demanding environment of 'real life' applications.

7. Conclusion

Implementation of photocatalysis for water treatment is challenging as it requires the design of robust and efficient photocatalysts both in terms of photocatalytic activity and in the ability to absorb a wide range of light. SP processes can address issues in terms of cost-effective access to defect-free, finely tuned catalysts at a large scale, the economic considerations being mostly dependent on the cost of the precursors. The self-sustained method, FSP, is more versatile because a wider range of precursors can be used to deliver nanostructured photocatalysts. In addition, FSP has recently been the object of exciting engineering developments which bring even more possibilities such as co-doping, direct anionic doping and separate tuning of metal oxide substrate and noble metal deposits.

Overall, there is great potential for SP-made noble metal based photocatalysts which offer improved activity under UV irradiation compared to bare TiO_2 counterparts as well as absorption of visible light *via* the plasmonic effect. However, the photocatalytic activity is also influenced by a set of parameters such as particle size, polymorph ratio, crystallinity, noble metal content and surface chemistry. More insights into the complex influence of these parameters will have to be gained to design improved noble metal/metal oxide photocatalysts in a rational way. SP processes could ultimately combine the ability to make complex composites and to directly deposit these onto suitable substrates resulting in a very efficient way of preparing photocatalytic components for reactors. As this review has highlighted, very little testing on FSP made thin films has been carried out as yet for water depollution and key characteristics such as film adhesion must be further investigated to provide durable composites for this application.

Acknowledgments

The authors thank Helen Gavin and Robert Potter for helpful comments and suggestions. This work has been supported by the European Commission funded 7th Framework Programme Project LIMPID (Grant No. 310177).

References

1. M. N. Chong, B. Jin, C. W. K. Chow and C. Saint, *Water Res.*, 2010, **44**, (10), 2997

2. K. Nagaveni, M. S. Hegde and G. Madras, *J. Phys. Chem. B*, 2004, **108**, (52), 20204
3. L. G. Devi and R. Kavitha, *Appl. Catal. B: Environ.*, 2013, **140–141**, 559
4. Y. Cho, W. Choi, C.-H. Lee, T. Hyeon and H.-I. Lee, *Environ. Sci. Technol.*, 2001, **35**, (5), 966
5. R. Leary and A. Westwood, *Carbon*, 2011, **49**, (3), 741
6. G.-S. Li, D.-Q. Zhang and J. C. Yu, *Environ. Sci. Technol.*, 2009, **43**, (18), 7079
7. S. Balachandran, N. Prakash, K. Thirumalai, M. Muruganandham, M. Sillanpää and M. Swaminathan, *Ind. Eng. Chem. Res.*, 2014, **53**, (20), 8346
8. X. Zhang, Y. L. Chen, R.-S. Liu and D. P. Tsai, *Rep. Prog. Phys.*, 2013, **76**, 046401
9. J. Yu, L. Yue, S. Liu, B. Huang and X. Zhang, *J. Colloid Interface Sci.*, 2009, **334**, (1), 58
10. S. C. Chan and M. A. Barteau, *Langmuir*, 2005, **21**, (12), 5588
11. L. Delannoy, N. E. Hassan, A. Musi, N. N. L. To, J.-M. Krafft and C. Louis, *J. Phys. Chem. B*, 2006, **110**, (45), 22471
12. M. C. Hidalgo, M. Maicu, J. A. Navío and G. Colón, *J. Phys. Chem. C*, 2009, **113**, (29), 12840
13. J. Fang, S.-W. Cao, Z. Wang, M. M. Shahjamali, S. C. J. Loo, J. Barber and C. Xue, *Int. J. Hydrogen Energy*, 2012, **37**, (23), 17853
14. W.-C. Li, M. Comotti and F. Schüth, *J. Catal.*, 2006, **237**, (1), 190
15. W. Y. Teoh, *Materials*, 2013, **6**, (8), 3194
16. W. Y. Teoh, R. Amal and L. Mädler, *Nanoscale*, 2010, **2**, (8), 1324
17. S. E. Pratsinis, *AIChE J.*, 2010, **56**, (12), 3028
18. R. Mueller, L. Mädler and S. E. Pratsinis, *Chem. Eng. Sci.*, 2003, **58**, (10), 1969
19. R. Mueller, R. Jossen, S. E. Pratsinis, M. Watson and M. K. Akhtar, *J. Am. Ceram. Soc.*, 2004, **87**, (2), 197
20. K. Kaneko, W.-J. Moon, K. Inoke, Z. Horita, S. Ohara, T. Adschiri, H. Abe and M. Naito, *Mater. Sci. Eng.: A*, 2005, **403**, (1–2), 32
21. S. Kozhukharov and S. Tchaoushev, *J. Chem. Technol. Metall.*, 2013, **48**, (1), 111
22. R. Strobel, A. Alfons and S. E. Pratsinis, *Adv. Powder Technol.*, 2006, **17**, (5), 457
23. S. G. Kumar and L. G. Devi, *J. Phys. Chem. A*, 2011, **115**, (46), 13211
24. M. A. Henderson, *Surf. Sci. Rep.*, 2011, **66**, (6–7), 185
25. V. Subramanian, E. E. Wolf and P. V. Kamat, *J. Am. Chem. Soc.*, 2004, **126**, (15), 4943
26. A. L. Linsebigler, G. Lu and J. T. Yates, *Chem. Rev.*, 1995, **95**, (3), 735
27. S. Sakthivel, M. V. Shankar, M. Palanichamy, B. Arabindoo, D. W. Bahnemann and V. Murugesan, *Water Res.*, 2004, **38**, (13), 3001
28. S. T. Kochuveedu, Y. H. Jang and D. H. Kim, *Chem. Soc. Rev.*, 2013, **42**, (21), 8467
29. L. Mädler, W. J. Stark and S. E. Pratsinis, *J. Mater. Res.*, 2003, **18**, (1), 115
30. R. Strobel and S. E. Pratsinis, *Platinum Metals Rev.*, 2009, **53**, (1), 11
31. W. Y. Teoh, L. Mädler, D. Beydoun, S. E. Pratsinis and R. Amal, *Chem. Eng. Sci.*, 2005, **60**, (21), 5852
32. W. Y. Teoh, L. Mädler and R. Amal, *J. Catal.*, 2007, **251**, (2), 271
33. V. Tiwari, J. Jiang, V. Sethi and P. Biswas, *Appl. Catal. A: Gen.*, 2008, **345**, (2), 241
34. I. E. Paulauskas, D. R. Modeshia, T. T. Ali, E. H. El-Mossalamy, A. Y. Obaid, S. N. Basahel, A. A. Al-Ghamdi and F. K. Sartain, *Platinum Metals Rev.*, 2013, **57**, (1), 32
35. A. B. Haugen, I. Kumakiri, C. Simon and M.-A. Einarsrud, *J. Eur. Ceram. Soc.*, 2011, **31**, (3), 291
36. M. J. Height, S. E. Pratsinis, O. Mekasuwandumrong and P. Praserthdam, *Appl. Catal. B: Environ.*, 2006, **63**, (3–4), 305
37. C. Siriwong, C. Liewhiran, N. Wetchakun and S. Phanichphant, 'Characterization and Photocatalytic Activity of Pd-doped ZnO Nanoparticles Synthesized by Flame Spray Pyrolysis', Nanoelectronics Conference, INEC 2008, 2nd IEEE International, Shanghai, China, 2008, pp. 869–874
38. P. Pawinrat, O. Mekasuwandumrong and J. Panpranot, *Catal. Commun.*, 2009, **10**, (10), 1380
39. K. L. Kelly, E. Coronado, L. L. Zhao and G. C. Schatz, *J. Phys. Chem. B.*, 2003, **107**, (3), 668
40. K. A. Willets and R. P. Van Duyne, *Ann. Rev. Phys. Chem.*, 2007, **58**, 267
41. A. Bumajdad and M. Madkour, *Phys. Chem. Chem. Phys.*, 2014, (16), 7146
42. B. Pongthawornsakun, S.-i. Fujita, M. Arai, O. Mekasuwandumrong and J. Panpranot, *Appl. Catal. A: Gen.*, 2013, **467**, 132
43. C. Gunawan, W. Y. Teoh, C. P. Marquis, J. Lifia and R. Amal, *Small*, 2009, **5**, (3), 341
44. C. Han, V. Likodimos, J. A. Khan, M. N. Nadagouda, J. Andersen, P. Falaras, P. Rosales-Lombardi and D. D. Dionysiou, *Environ. Sci. Pollut. Res.*, 2014, **21**,

(20), 11781

45. S. Kaviya and E. Prasad, *RSC Advances*, 2015, **5**, (22), 17179
46. S. Hannemann, J.-D. Grunwaldt, F. Krumeich, P. Kappen and A. Baiker, *Appl. Surf. Sci.*, 2006, **252**, (22), 7862
47. G. A. Sotiriou, G. D. Etterlin, A. Spyrogianni, F. Krumeich, J.-C. Leroux and S. E. Pratsinis, *Chem. Commun.*, 2014, **50**, (88), 13559
48. A. Zielińska-Jurek, E. Kowalska, J. W. Sobczak, W. Lisowski, B. Ohtani and A. Zaleska, *Appl. Catal. B: Environ.*, 2011, **101**, (3–4), 504
49. H. Schulz, L. Mädler, R. Strobel, R. Jossen, S. E. Pratsinis and T. Johannessen, *J. Mater. Res.*, 2005, **20**, (9), 2568
50. J.-M. Herrmann, *New J. Chem.*, 2012, **36**, (4), 883
51. F. Zuo, L. Wang, T. Wu, Z. Zhang, D. Borchardt and P. Feng, *J. Am. Chem. Soc.*, 2010, **132**, (34), 11856
52. M. S. Hamdy, R. Amrollahi and G. Mul, *ACS Catal.*, 2012, **2**, (12), 2641
53. Q. Zhu, Y. Peng, L. Lin, C.-M. Fan, G.-Q. Gao, R.-X. Wang and A.-W. Xu, *J. Mater. Chem. A*, 2014, **2**, (12), 4429
54. A. Naldoni, M. Allieta, S. Santangelo, M. Marelli, F. Fabbri, S. Cappelli, C. L. Bianchi, R. Psaro and V. Dal Santo, *J. Am. Chem. Soc.*, 2012, **134**, (18), 7600
55. Y. Yang, T. Zhang, L. Le, X. Ruan, P. Fang, C. Pan, R. Xiong, J. Shi and J. Wei, *Sci. Rep.*, 2014, **4**, 7045
56. Y. K. Kho, W. Y. Teoh, L. Mädler and R. Amal, *Chem. Eng. Sci.*, 2011, **66**, (11), 2409
57. A. Teleki and S. E. Pratsinis, *Phys. Chem. Chem. Phys.*, 2009, **11**, (19), 3742
58. K. Wegner and S. E. Pratsinis, *AIChE J.*, 2003, **49**, (7), 1667
59. J. Huo, Y. Hu, H. Jiang and C. Li, *Nanoscale*, 2014, **6**, (15), 9078
60. S. J. Tauster, *Acc. Chem. Res.*, 1987, **20**, (11), 389
61. K. Fujiwara, Y. Deligiannakis, C. G. Skoutelis and S. E. Pratsinis, *Appl. Catal. B: Environ.*, 2014, **154–155**, 9
62. M. V. Dozzi, G. L. Chiarello and E. Selli, *J. Adv. Oxid. Technol.*, 2010, **13**, (3), 305
63. R. Marschall and L. Wang, *Catal. Today*, 2014, **225**, 111
64. D. Li, H. Haneda, N. K. Labhsetwar, S. Hishita and N. Ohashi, *Chem. Phys. Lett.*, 2005, **401**, (4–6), 579
65. D. Li, N. Ohashi, S. Hishita, T. Kolodiazhnyi and H. Haneda, *J. Solid State Chem.*, 2005, **178**, (11), 3293
66. J. C. Yu, W. Ho, J. Yu, H. Yip, P. K. Wong and J. Zhao, *Environ. Sci. Technol.*, 2005, **39**, (4), 1175
67. H. Liu and L. Gao, *J. Am. Ceram. Soc.*, 2004, **87**, (8), 1582
68. R. Asahi, T. Morikawa, T. Ohwaki, K. Aoki and Y. Taga, *Science*, 2001, **293**, (5528), 269
69. J. Zhang, Y. Wu, M. Xing, S. A. K. Leghari and S. Sajjad, *Energy Environ. Sci.*, 2010, **3**, (6), 715
70. V. Etacheri, M. K. Seery, S. J. Hinder and S. C. Pillai, *Chem. Mater.*, 2010, **22**, (13), 3843
71. D. Dolat, S. Mozia, B. Ohtani and A. W. Morawski, *Chem. Eng. J.*, 2013, **225**, 358
72. Y. Jiang, J. Scott and R. Amal, *Appl. Catal. B: Environ.*, 2012, **126**, 290
73. G. L. Chiarello, M. V. Dozzi, M. Scavini, J.-D. Grunwaldt and E. Selli, *Appl. Catal. B: Environ.*, 2014, **160–161**, 144
74. J. Huo, Y. Hu, H. Jiang, X. Hou and C. Li, *Chem. Eng. J.*, 2014, **258**, 163
75. R. Strobel, L. Mädler, M. Piacentini, M. Maciejewski, A. Baiker and S. E. Pratsinis, *Chem. Mater.*, 2006, **18**, (10), 2532
76. M. Høj, D. K. Pham, M. Brorson, L. Mädler, A. D. Jensen and J.-D. Grunwaldt, *Catal. Lett.*, 2013, **143**, (5), 386
77. H. K. Grossmann, T. Grieb, F. Meierhofer, M. J. Hodapp, D. Noriler, A. Gröhn, H. F. Meier, U. Fritsching, K. Wegner and L. Mädler, *J. Nanopart. Res.*, 2015, **17**, (4), 1
78. A. Y. Shan, T. I. M. Ghazi and S. A. Rashid, *Appl. Catal. A: Gen.*, 2010, **389**, (1–2), 1
79. P. Du, J. T. Carneiro, J. A. Moulijn and G. Mul, *Appl. Catal. A: Gen.*, 2008, **334**, (1–2), 119
80. H. Dzinun, M. H. D. Othman, A. F. Ismail, M. H. Puteh, M. A. Rahman and J. Jaafar, *Chem. Eng. J.*, 2015, **269**, 255
81. M. A. Lazar, S. Varghese and S. S. Nair, *Catalysts*, 2012, **2**, (4), 572
82. C. J. Brinker and M. S. Harrington, *Sol. Energy Mater.*, 1981, **5**, (2), 159
83. G. San Vicente, A. Morales and M. T. Gutierrez, *Thin Solid Films*, 2001, **391**, (1), 133
84. Q. Fan, B. McQuillin, A. K. Ray, M. L. Turner and A. B. Seddon, *J. Phys. D: Appl. Phys.*, 2000, **33**, (21), 2683
85. G. A. Battiston, R. Gerbasi, M. Porchia and A. Marigo, *Thin Solid Films*, 1994, **239**, (2), 186
86. D.-J. Won, C.-H. Wang, H.-K. Jang and D.-J. Choi, *Appl. Phys. A*, 2001, **73**, (5), 595
87. P. Löbl, M. Huppertz and D. Mergel, *Thin Solid Films*,

1994, **251**, (1), 72

88. L.-J. Meng and M. P. dos Santos, *Thin Solid Films*, 1993, **226**, (1), 22
89. N. Martin, C. Rousselot, C. Savall and F. Palmino, *Thin Solid Films*, 1996, **287**, (1–2), 154
90. K. Okimura, *Surf. Coat. Technol.*, 2001, **135**, (2–3), 286
91. M. P. Moret, R. Zallen, D. P. Vijay and S. B. Desu, *Thin Solid Films*, 2000, **366**, (1–2), 8
92. L. Kavan and M. Grätzel, *Electrochim. Acta*, 1995, **40**, (5), 643
93. P. S. Shinde, S. B. Sadale, P. S. Patil, P. N. Bhosale, A. Brüger, M. Neumann-Spallart and C. H. Bhosale, *Sol. Energy Mater. Sol. Cells*, 2008, **92**, (3), 283
94. T. Thiwawong, K. Onlaor and B. Tunhoo, *Adv. Mater. Sci. Eng.*, 2013, 640428
95. G. Varshney, S. R. Kanel, D. M. Kempisty, V. Varshney, A. Agrawal, E. Sahle-Demessie, R. S. Varma and M. N. Nadagouda, *Coord. Chem. Rev.*, 2016, **306**, (1), 43
96. Z.-M. Wang, E. Sahle-Demessie, A. Aly Hassan and C. Perrett, *J. Environ. Eng.*, 2012, **138**, (9), 923
97. B. Schimmoeller, H. Schulz, S. E. Pratsinis, A. Bareiss, A. Reitzmann and B. Kraushaar-Czarnetzki, *J. Catal.*, 2006, **243**, (1), 82
98. E. Diler, S. Rioual, B. Lescop, D. Thierry and B. Rouvellou, *Thin Solid Films*, 2012, **520**, (7), 2819
99. A. Tricoli, M. Righettoni and S. E. Pratsinis, *Langmuir*, 2009, **25**, (21), 12578
100. A. Tricoli, M. Graf, F. Mayer, S. Kuühne, A. Hierlemann and S. E. Pratsinis, *Adv. Mater.*, 2008, **20**, (16), 3005
101. R. Kavitha, S. Meghani and V. Jayaram, *Mater. Sci. Eng.: B*, 2007, **139**, (2–3), 134
102. R. Strobel and S. E. Pratsinis, *J. Mater. Chem.*, 2007, **17**, (45), 4743
103. K. Wegner, S. Vinati, P. Piseri, A. Antonini, A. Zelioli, E. Barborini, C. Ducati and P. Milani, *Nanotechnology*, 2012, **23**, (18), 185603
104. H. Keskinen, J. M. Mäkelä, M. Aromaa, J. Keskinen, S. Areva, C. V. Teixeira, J. B. Rosenholm, V. Pore, M. Ritala, M. Leskelä, M. Raulio, M. S. Salkinoja-Salonen, E. Levänen and T. Mäntylä, *Catal. Lett.*, 2006, **111**, (3), 127
105. L. Mädler, A. Roessler, S. E. Pratsinis, T. Sahm, A. Gurlo, N. Barsan and U. Weimar, *Sens. Actuators B: Chem.*, 2006, **114**, (1), 283
106. S. Thybo, S. Jensen, J. Johansen, T. Johannessen, O. Hansen and U. J. Quaade, *J. Catal.*, 2004, **223**, (2), 271
107. D. Perednis and L. J. Gauckler, *J. Electroceram.*, 2005, **14**, (2), 103
108. C. Guild, S. Biswas, Y. Meng, T. Jafari, A. M. Gaffney and S. L. Suib, *Catal. Today*, 2014, **238**, 87
109. V. Iliev, D. Tomova, R. Todorovska, D. Oliver, L. Petrov, D. Todorovsky and M. Uzunova-Bujnova, *Appl. Catal. A: Gen.*, 2006, **313**, (2), 115
110. N. L. Tarwal and P. S. Patil, *Electrochim. Acta*, 2011, **56**, (18), 6510
111. V. S. Mohite, M. A. Mahadik, S. S. Kumbhar, Y. M. Hunge, J.-H. Kim, A. V. Moholkar, K. Y. Rajpure and C. H. Bhosale, *J. Photochem. Photobiol. B: Biol.*, 2015, **142**, 204
112. I. O. Acik, L. Dolgov, M. Krunks, A. Mere, V. Mikli, S. Pikker, A. Loot and I. Sildos, *Thin Solid Films*, 2014, **553**, 144
113. I. O. Acik, N. G. Oyekoya, A. Mere, A. Loot, L. Dolgov, V. Mikli, M. Krunks and I. Sildos, *Surf. Coat. Technol.*, 2015, **271**, 27

The Authors

Dr Frédéric Pelletier received his PhD in organometallic and coordination chemistry from the University of Toulouse, France, in 2012 and subsequently joined Johnson Matthey Technology Centre, Sonning Common, UK, as a Research Scientist. His research activity concerns the synthesis of nanomaterials with controlled morphology and their use in heterogeneous catalysis and environmental applications.

Dr Bénédicte Thiébaut joined Johnson Matthey in 1999 and worked on numerous projects specialising in the nanotechnology area. She initially investigated the synthesis of nanomaterials by solution routes and turned her interest to other methodologies including the flame spray pyrolysis technique.

